218 *Chem. Mater.* **2010,** *22,* 218–225
DOI:10.1021/cm902770d

CHEMISTRY OF MATERIALS
Article

ZnO Nanostructures Grown onto Polypyrrole Films Prepared in Swollen Liquid Crystals via Integrative Chemistry

Dong Un Lee,[†] Debabrata Pradhan,[‡] Rola Mouawia,[†] Doo Hwan Oh,[†] Nina F. Heinig,[‡] Kam Tong Leung,[‡] and Eric Prouzet*,[†]

[†]*Chemistry & Waterloo Institute of Nanotechnology, University of Waterloo, 200 University Av. West, Waterloo, Ontario N2L 3G1, Canada and* [‡]*Chemistry & WatLab, University of Waterloo, 200 University Av. West, Waterloo, Ontario N2L 3G1, Canada*

Received September 4, 2009. Revised Manuscript Received November 7, 2009

We report the synthesis of ZnO nanostructures via electrodeposition onto films of polypyrrole (PPy) obtained by an electroless method from an aqueous suspension of PPy nanosheets. The PPy nanosheets are initially prepared in hexagonal oil-in-water (o/w) swollen liquid crystal (SLC) to provide the lamellar structure required to achieve further formation of a smooth electrode by an electroless process. The PPy particles can be easily extracted and transferred into an aqueous suspension that can be stored for months until its final use. The aqueous suspension of PPy is further spin-coated onto a glass or silicon substrate to form a flat thin film. These films exhibit a significant conductivity that allows further growth of various zinc oxide nanostructures by electrodeposition.

Introduction

Semiconducting nanostructures are promising materials that can be inserted as smart materials into microsystems and provide various functions, such as application as nanogenerators, electron emitters, or sensors.[1] Among semiconducting nanostructures, zinc oxide (ZnO) offers many assets including numerous geometries that emphasize specific properties.[2] These nanostructures can be generated by electrodeposition with parameters (concentration, potential, ...) that can be modified to achieve the formation of different nanostructures.[3] The formation of such nanostructures has been confirmed by different studies but there are still challenges to apply these methods to large deposition processes onto inexpensive conductive supports such as plastic films or to create specific patterns generated at the micrometric or nanometric range. This requires that the electrodeposition of ZnO must follow a preliminary deposition of a conducting material that will direct the further growth of ZnO. For the first application, spray drying of this conducting material would be a solution whereas inkjet printing would allow a very versatile production of patterned nanostructures and rapid prototyping.[4] Both applications require that a wet suspension of a conducting material could be achieved, with particle shapes that would allow the formation of smooth films.

In the following, we report how the preparation of polypyrrole (PPy), which is a well-known conducting polymer, can be achieved with a process that constitutes the first step toward the further fabrication of large surface electrodes or conductive patterns. This method is illustrated by the synthesis of zinc oxide nanostructures onto PPy thin films prepared by spin coating. Polypyrrole has been studied either as a conductive substrate or as an intrinsic chemical sensor.[5] PPy can be synthesized by electrochemical methods; however, this method does not favor the formation of large surface area or good patterning and surfaces generally obtained by electrochemical deposition exhibit a rather high roughness. Depending on methods, polypyrrole was obtained with various shapes including thin layer, opened porous structure or nanoparticles.[6] It has been also designed to facilitate its integration into nanocomposites.[7,8] Specific

*Author to whom correspondence should be addressed. E-mail: eprouzet@scimail.uwaterloo.ca.

(1) Wang, Z. L.; Song, J. *Science* **2006**, *312*, 242.
(2) Gao, P. X.; Lao, C. S.; Ding, Y.; Wang, Z. L. *Adv. Funct. Mater.* **2006**, *16*, 53.
(3) Pradhan, D.; Kumar, M.; Ando, Y.; Leung, K. T. *J. Phys. Chem. C* **2008**, *112*, 7093.
(4) (a) Shah, P.; Kevrekidis, Y.; Benziger, J. *Langmuir* **1999**, *15*, 1584. (b) Fan, H.; Lu, Y.; Stump, A.; Reed, S. T.; Baer, T.; Schunk, R.; Perez-Luna, V.; Lopez, G. P.; Brinker, C. J. *Nature* **2000**, *405*, 56. (c) Magdassi, S.; Ben Moshe, M. *Langmuir* **2003**, *19*, 939. (d) Park, J.; Moon, J. *Langmuir* **2006**, *22*, 3506. (e) Park, B. K.; Kim, D.; Jeong, S.; Moon, J.; Kim, J. S. *Thin Solid Films* **2007**, *515*, 7706. (f) Huber, J.; Amgoune, A.; Mecking, S. *Adv. Mater.* **2008**, *20*, 1978. (g) Kumar, B.; Tan, H. S.; Ramalingam, N.; Mhaisalkar, S. G. *Carbon* **2009**, *47*, 321. (h) Lejeune, M.; Chartier, T.; Dossou-Yovo, C.; Noguera, R. *J. Eur. Ceram. Soc.* **2009**, *29*, 905.
(5) Saunders, B. R.; Fleming, R. J.; Murray, K. S. *Chem. Mater.* **1995**, *7*, 1082.
(6) (a) Dai, T.; Lu, Y. *J. Mater. Chem.* **2007**, *17*, 4797. (b) Intelmann, C. M.; Syritski, V.; Tsankov, D.; Hinrichs, K.; Rappich, J. *Electrochim. Acta* **2008**, *53*, 4046. (c) Sohn, D.; Moon, H.; Fasolka, M. J.; Eidelman, N.; Koo, S.-M.; Richter, C. A.; Park, S.; Kopanski, J. J.; Amis, E. *Chem. Lett.* **2007**, *36*, 210.
(7) (a) Feng, C. Q.; Chew, S. Y.; Guo, Z. P.; Wang, J. Z.; Liu, H. K. *J. Power Sources* **2007**, *174*, 1095–1099. (b) Green, R. A.; Williams, C. M.; Lovell, N. H.; Poole-Warren, L. A. *J. Mater. Sci.: Mater. Med.* **2008**, *19*, 1625. (c) Guo, H.; Zhu, H.; Lin, H.; Zhang, J. *Colloid Polym. Sci.* **2008**, *286*, 587.
(8) (a) Kim, J.-Y.; Kim, K. H.; Kim, K. B. *J. Power Sources* **2008**, *176*, 396. (b) Min, H.-S.; Park, B. Y.; Taherabadi, L.; Wang, C.; Yeh, Y.; Zaouk, R.; Madou, M. J.; Dunn, B. *J. Power Sources* **2008**, *178*, 795–800. (c) Reddy, A. L. M.; Rajalakshmi, N.; Ramaprabhu, S. *Carbon* **2008**, *46*, 2. (d) Ren, L.; Wang, L.; Zhang, F. *Rare Met.* **2007**, *26*, 591. (e) Yuan, L.; Wang, J.; Chew, S. Y.; Chen, J.; Guo, Z. P.; Zhao, L.; Konstantinov, K.; Liu, H. K. *J. Power Sources* **2007**, *174*, 1183.

 Published on Web 11/20/2009

shaping of PPy could be achieved using solid porous matrices as molds that confine the polymer reaction in their porous network.[9] Surface reaction were also studied,[10] and nanofibers were synthesized directly by a seed-induced bulk polymerization.[11,12] However, the major drawback of the hard template methods is the further recovery of the polymer, which implies total dissolution of the solid matrix. It has been demonstrated in parallel that dynamic soft matrices can overcome this problem with the additional potential that they can be recovered and recycled in the process. This was first illustrated by the use of binary liquid crystals (LCs) for the synthesis of mesoporous platinum and silica films.[13] We extended this concept to complex systems described as hexagonal oil-in-water (o/w) swollen liquid crystals (SLCs). These mesophases, which were discovered initially by L. Ramos, are the perfect example of dynamic molds that can be tuned for a versatile chemistry.[14,15] They can be tuned by changing the oil:water ratio over a large range, leading to cell parameters varying from 3 nm to 30 nm, and they exhibit a high anisotropy, because of their hexagonal symmetry. Finally, they can be easily destabilized after reaction to recover the final product. Moreover, unlike binary LCs, they possess both organic and aqueous phases that allow a wide variety of materials to be synthesized within.[15−18]

To our knowledge, the synthesis of PPy in soft molds has been reported only with ionic liquids.[19] Therefore, we have applied the method developed with SLCs to the synthesis of PPy in the aqueous phase. The specific structure of SLC allowed us to obtain PPy nanosheets that can be recovered and stored before being used for the formation of electrodes. Their specific shape facilitates their further merging in a continuous structure when they are deposited onto a substrate. This first report focuses on the synthesis of the PPy particles and how they can be further used to generate electrodes onto which ZnO nanostructures are synthesized by electrodeposition. We demonstrate the ability of these nanosheets to form continuous and very smooth film using spin-coating deposition methods onto isolating supports (glass slide or silicon wafer). This general process, which combines concepts and methods from soft chemistry, sol−gel methods, biomimetic reactions, and soft matter systems, illustrates perfectly the concept of integrative chemistry (IC), which provides the final complexity of integrated structures by the "multiplexing" operation of single chemical and physicochemical processes.[20]

Experimental Section

Synthesis of ZnO Nanostructures. All reagents were used as received. Electrodeposition of ZnO onto PPy thin film was performed at two concentrations of $Zn(NO_3)_2 \cdot 6H_2O$ (Aldrich): 0.001 M and 0.1 M. The PPy films, used as substrates, were prepared by spin coating onto silicon wafer substrates. The electrochemical deposition was conducted in a three-electrode glass cell immersed in a water bath held at 60 °C. The working electrode was the single-sided PPy spin-coated silicon wafer. An Ag/AgCl electrode was used as the reference, and platinum wire was used as the counter electrode. Fifteen milliliters of a 0.001 M or 0.1 M aqueous solution of $Zn(NO_3)_2 \cdot 6H_2O$ (Aldrich) was used as the electrolyte and mixed with a 0.1 M KCl (EMD) solution as the supporting electrolyte for the electrochemical deposition. The exposed dimensions of the working electrode were ~5 mm × ~3 mm. A potentiogalvanostatic electrochemical workstation (CH Instruments 440) was used to deposit the nanostructures via amperometry with a potential set at −0.9 V (relative to the Ag/AgCl reference electrode) with a deposition time of 1 h. After deposition, the resulting film was thoroughly rinsed with Millipore water and dried under a nitrogen gas stream. The nanostructures obtained were compared with materials obtained with same parameters but deposited onto gold-coated silicon wafers and spin-coated PPy films prepared onto gold-coated silicon wafers, to understand how the film conductivity could disturb the ZnO deposition.

Characterization. Dynamic light scattering (DLS) analyses were performed with a Cordouan DL135 particle size analyzer set at 30 °C, with a laser wavelength of 650 nm and a static detector set at an angle of 135° from the incident beam. The average counting intensity was set at ~6000 kHz by tuning the laser intensity, except for the more-diluted samples (20%), where only a maximum intensity of 2000 kHz could be obtained. For each sample, several records were obtained by varying the time of

(9) (a) Ikegame, M.; Tajima, K.; Aida, T. *Angew. Chem., Int. Ed.* **2003**, *42*, 2154. (b) He, J.; Chen, W.; Xu, N.; Li, L.; Li, X.; Xue, G. *Appl. Surf. Sci.* **2004**, *221*, 87. (c) Kumar, S.; Kumar, S.; Chakarvarti, S. K. *Phys. Lett. A* **2004**, *327*, 198. Lee, A. S.; Peteu, S. F.; Ly, J. V.; Requicha, A. A. G.; Thompson, M. E.; Zhou, C. *Nanotechnology* **2008**, *19*, 165501.
(10) (a) Zhang, W.; Wen, X.; Yang, S. *Langmuir* **2003**, *19*, 4420. (b) Li, M.; Yuan, J.; Shi, G. *Thin Solid Films* **2008**, *516*, 3836. (c) Mtsuko, D.; Avnon, A.; Lievonen, J.; Ahlskog, M.; Menon, R. *Nanotechnology* **2008**, *19*, 125304.
(11) Zhang, X.; Manohar, S. K. *J. Am. Ceram. Soc.* **2004**, *126*, 12714.
(12) Athawale, A. A.; Katre, P. P.; Bhagwat, S. V.; Dhamane, A. H. *J. Appl. Polym. Sci.* **2008**, *108*, 2872.
(13) (a) Attard, G. S.; Glyde, J. C.; Göltner, C. G. *Nature* **1995**, *378*, 366. (b) Attard, G. S.; Bartlett, P. N.; Coleman, N. R. B.; Elliott, J. M.; Owen, J. R.; Wang, J. H. *Science* **1997**, *278*, 838. (c) Attard, G. S.; Göltner, C. G.; Corker, J. M.; Henke, S.; Templer, R. H. *Angew. Chem., Int. Ed.* **1997**, *36*, 1315.
(14) Ramos, L.; Fabre, P. *Langmuir* **1997**, *13*, 682.
(15) Surendran, G.; Tokumoto, M.; Pena dos Santos, E.; Remita, H.; Ramos, L.; Kooyman, P. J.; Santilli, C. V.; Bourgaux, C.; Dieudonné, P.; Prouzet, E. *Chem. Mater.* **2005**, *17*, 1505.
(16) (a) Pena dos Santos, E.; Santilli, C. V.; Pulcinelli, S. H.; Prouzet, E. *Chem. Mater.* **2004**, *16*, 4187. (b) Surendran, G.; Apostolescu, G.; Tokumoto, M.; Prouzet, E.; Ramos, L.; Beaunier, P.; Kooyman, P. J.; Etcheberry, A.; Remita, H. *Small* **2005**, *1*, 964. (c) Surendran, G.; Ksar, F.; Ramos, L.; Keita, B.; Nadjo, L.; Prouzet, E.; Beaunier, P.; Dieudonné, P.; Audonnet, F.; Remita, H. *J. Phys. Chem. C* **2008**, *112*, 10740.
(17) Pena dos Santos, E.; Tokumoto, M.; Surendran, G.; Remita, H.; Bourgaux, C.; Dieudonné, P.; Prouzet, E.; Ramos, L. *Langmuir* **2005**, *21*, 4362.
(18) Surendran, G.; Ramos, L.; Pansu, B.; Prouzet, E.; Beaunier, P.; Audonnet, F.; Remita, H. *Chem. Mater.* **2007**, *19*, 5045.
(19) Kim, J.-Y.; Kim, J.-T.; Song, E.-A.; Min, Y.-K.; Hamaguchi, H.-o. *Macromolecules* **2008**, *41*, 2886.
(20) (a) Backov, R. *Soft Matter* **2006**, *2*, 452. (b) Prouzet, E.; Ravaine, S.; Sanchez, C.; Backov, R. *New J. Chem.* **2008**, *32*, 1284. (c) Boissière, C.; Grosso, D.; Prouzet, E. In *Nanomaterials: Inorganic and Bioorganic Perspectives*; Luckehart, C. M., Scott, R. A., Eds.; Johm Wiley & Sons, Ltd: Chichester, U.K., 2008; Vol. *2*.

recording, the range of calculation of the autocorrelation function, and the unit time range ($\delta\tau$). The particle size distribution was calculated using a Padé−Laplace model, to take into account possible polydispersity.[21] We ran several analyses for each sample (from 20% to 100%) to obtain a statistical evaluation of the average size. However, it is worth mentioning that the numerical values obtained by this method are the hydrodynamic diameters of the particles calculated from the Stokes−Einstein equation, which can differ from its actual size, especially with lamellar shapes. Scanning electron microscopy (SEM) images were obtained with a Leo Model 1530 FEG microscope (WATLAB, University of Waterloo). Preparation of the SEM samples was performed using natural drying of a drop of the aqueous suspension on a silicon substrate or direct observation of the PPy thin films obtained by spin coating, as well as ZnO nanstructures. All samples were gold-coated beforehand. Atomic force microscopy (AFM) data were obtained in tapping mode, with a Digital Instrument-Veeco Nanoman AFM system. The silicon tip had a nominal radius of curvature of ~10 nm. XRD of the PPy thin films was obtained in grazing incidence mode, using a Pan Analytical X'Pert-PRO diffractometer adapted for grazing incidence measurements and Cu Kα X-ray wavelength. Because of their large broadening, the diffraction peaks, which are usually fitted with pseudo-Voigt or Pearson VII functions, could be fitted by Gaussian curves once, after the background has been subtracted by a polynomial fit. Electrical conductivity measurement was achieved with a four-contacts measurement on a thick film of PPy spin-coated onto a glass slide. Contact was made using 0.1-mm silver wires (Alfa Aesar) set ~0.125 cm apart and lightly touching silver spots (0.05 cm in diameter) that were made of a silver paste. The measurement was done at room temperature using a Keithley Model 2400 SourceMeter, with four probes and a compliance voltage of 121 V. The sample was tested for electrical conductivity by applying DC current through the sample and measuring the output voltage using the SourceMeter.

Results and Discussion

Synthesis of Polypyrrole. All reagents were used as received. The synthesis of PPy in water was based on a method that was reported by Zhang et al., where PPy is obtained by the oxidation of pyrrole with ammonium peroxidisulfate. In the following, the synthesis of bulk PPy in pure water was performed accordingly, as for the synthesis in bulk water.[11]

Hexagonal SLCs are oil-in-water (o/w) LCs with surfactant-based cylinders that contain the oil phase, arranged in a hexagonal stacking in the continuous aqueous phase. SLCs are quaternary systems made of salted water, oil (cyclohexane), ionic surfactant, and a co-surfactant (1-pentanol).[14,15] The addition of salt is required to reach a given ionic force that will partially neutralize the electrostatic repulsion between the ionic surfactant heads. Its concentration is dependent on the curvature of cylinders (that is, on the amount of oil used to swell these cylinders). Any type of salt can be used, or it can be substituted by one of the precursors of the expected reaction.[14,17,18] Because it is important to keep the SLC stable during the reaction between pyrrole and catalyst, we proceeded via an interfacial reaction between one liquid crystal (A) stabilized with NaF and containing pyrrole dissolved in the aqueous phase and another (B) that has ammonium peroxidisulfate in place of NaF. The reaction proceeds through diffusion of the species in the aqueous frameworks of both phases while the entire mesophases remain intact.

Phase A was prepared with 1.14 g of cetyltrimethylammonium bromide (CTAB) added to a test tube with 2 mL of a solution of HCl (M) containing 0.025 g of NaF ([NaF] = 0.3 M).[15] Five mL of cyclohexane were further added to the tube. The tube was stirred with a vortex mixer until a well-dispersed, but unstable, milky emulsion was formed. Approximately 0.25 g of 1-pentanol was further added dropwise, in parallel with vortex stirring, until the entire solution become viscous and clear, as a proof of the formation of the SLC.[17] The correct amount of pentanol must be adjusted to the highest viscosity obtained, because any further addition will shift the entire system to a less-viscous spongelike structure. Phase A was enriched in pyrrole prior to the addition of pentanol. The amount of pyrrole was adjusted to the concentration reported initially by Zhang, that is, 2 mL of pyrrole added into the 2 mL of water ([Py] = 0.24 M).[11] In the following, this concentration will be noted as the "100%" sample and all other preparations noted as 20%−80%, accordingly. Different syntheses were performed with 80%, 60%, 40%, and 20% pyrrole, and their parameters are given in Table SI.1 in the Supporting Information. Phase B was prepared with 1.14 g of CTAB added to a test tube with 2 mL of HCl (M), 0.068 g of ammonium peroxidisulfate in place of NaF, and 0.21 g of 1-pentanol adjusted dropwise. In the following, except when specified, all results refer to the 100% sample ([Py] = 0.24 M in phase A).

The reaction was performed by bringing the two phases A and B into contact with each other, by pouring one phase (B) gently above the other one (A), to prevent any natural mixing and let the reaction occur by natural diffusion within the new SLC obtained, via the merging of phases A and B (see Figure 1a). Note that the rapid mixing of phases A and B using the vortex stirrer led to a rapid change of color: the solution turned almost immediately black, as proof of the formation of PPy. With the interfacial reaction, a black front appearing at the interface of phase A (bottom) and B (top) and progressively growing up into phase B, as a result of a diffusion of pyrrole—probably because of its lower density—through the aqueous network into the phase that contains the oxidant, where it formed PPy. This reaction did not disturb the mesophases that remained viscous, even after several weeks (see top of Figure 1b). The reaction was

(21) (a) Aubard, J.; Levoir, P.; Denis, A.; Claverie, P. *Comput. Chem.* **1987**, *11*, 163. (b) Bajzer, Z.; Myers, A. C.; Sedarous, S. S.; Prendergast, F. G. *Biophys. J.* **1989**, *56*, 79.

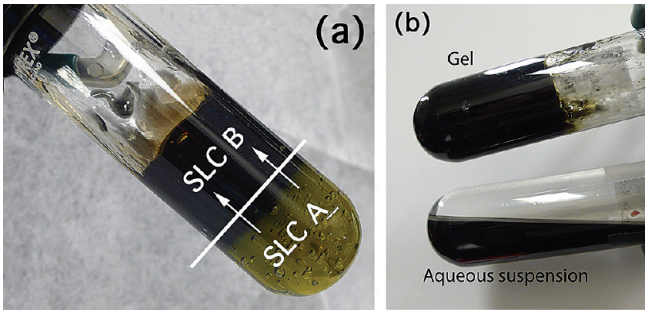

Figure 1. Formation of PPy in the swollen liquid crystal: (a) interfacial reaction between the SLC containing the pyrrole (A) and the SLC containing the catalyst (B); (b) final gel obtained at the end of the reaction (top) and the aqueous suspension of PPy nanoparticles obtained after extraction (bottom). As the reaction progresses, a black front appears at the interface of phase A (bottom) and B (top) and grows up into phase B, as a result of a diffusion of pyrrole through the aqueous network into the phase containing the oxidant where it formed PPy.

allowed to proceed for one week before the PPy were extracted and transferred into an aqueous solution (see bottom of Figure 1b).

The PPy particles were extracted according to the following process. First, the SLC was destabilized with a large excess of water (water:SLC = 3:1 (by volume)). Then, 15 mL of this solution was stirred with 15 mL of ethanol and centrifuged (1000 rpm, for 6 min), leading to a phase separation with a greenish-black top-layer that contains the PPy particles. This part was recovered and added to 15 mL of water and 15 mL of EtOH, sonicated for 5 min and centrifuged at 3000 rpm for 10 min. Particles of PPy segregate at the surface and can be recovered easily. They were redispersed in 10 mL of water acidified with HCl (pH 2), to protonate the polymer and facilitate its dispersion. The colloidal suspension is sonicated for 5 min and stored. Precipitation of PPy particles occurs only after several days, and they can be easily redispersed by hand shaking or short sonication.

Spin coating was performed with a Model P-6000 spin coater (SCS, Inc.) onto microscope glass slides or silicon wafers. The substrates were first cleaned and rinsed with ethanol (EtOH). Samples for conductivity measurements were prepared onto glass slides, because this process allowed us to obtain thicker films. Films were prepared with the aqueous suspension obtained from the 100% PPy sample at 1700 rpm, 75% speed ramp, and a spinning time of 120 s. After each spin coating of PPy thin film, the sample was left in an oven at ~35 °C, to ensure drying of the PPy film before repeating the coating process. For conductivity measurements, this process was repeated 10 times and the sample was cut into a 1 cm × 1 cm piece, using a diamond cutting pencil. Thin films prepared for analysis and ZnO electrodeposition were prepared onto silicon wafers. The silicon wafer was spin-coated at 4500 rpm for 60 s. A drop of suspension of PPy (100% sample) was dispensed as soon as the silicon wafer reached its maximum speed. The sample was left drying at room temperature for 15 min.

PPy particles prepared in bulk water appear as a homogeneous population of globular particles with an average size lying between 100 nm and 1.0 μm (see Figure 2).

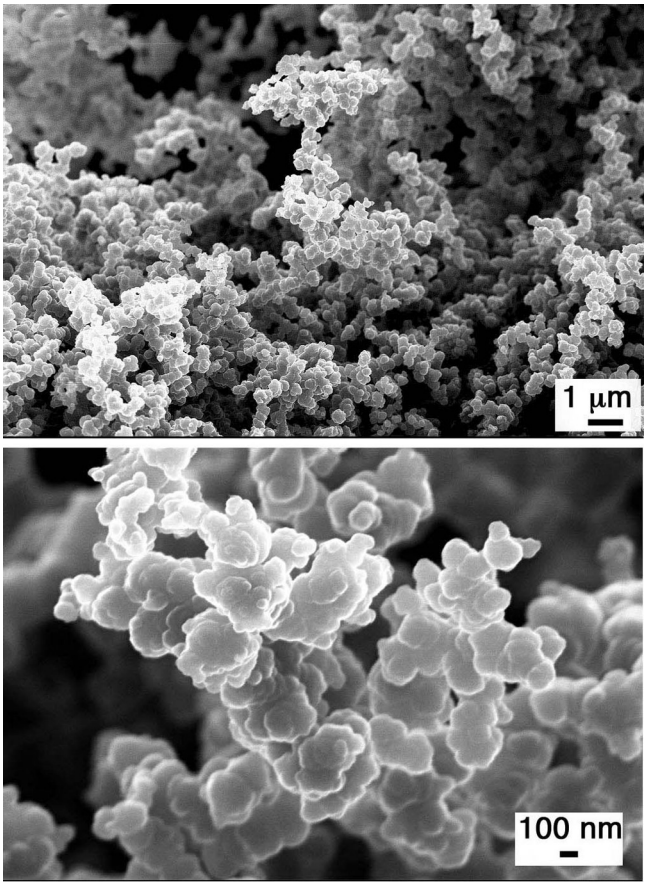

Figure 2. SEM micrographs of PPy prepared in bulk water. PPy particles prepared in bulk water appear as a homogeneous population of globular particles, with an average size lying between 100 nm and 1.0 μm.

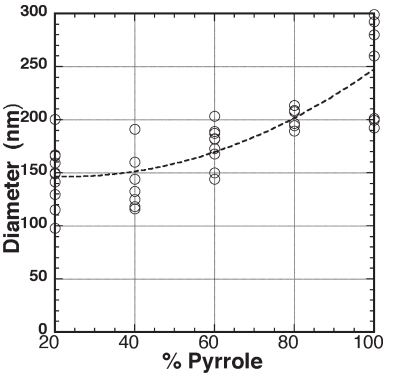

Figure 3. Hydrodynamic diameters deduced from the fit of the autocorrelation functions obtained from DLS analysis of the aqueous colloidal suspension of PPy particles synthesized in the swollen liquid crystals by interfacial reaction and allowed to react for 3 months. The size evolution was fitted by a second-degree polynomial for visual help. The term "100%" refers to an initial concentration of pyrrole that is equal to 0.24 M in phase A. The population of PPy particles remains rather monodisperse and nanometric, with an average hydrodynamic diameter that increases slightly from 150 nm to 300 nm as the amount of pyrrole increases from 20% to 100%.

A parallel analysis by DLS confirmed this observation with a mean size of 540 nm deduced from the autocorrelation function. (See Figure SI.1 in the Supporting Information.) Colloidal particles synthesized in the SLC were analyzed by DLS after extraction in the aqueous suspension. Figure 3 displays the evolution of the hydrodynamic

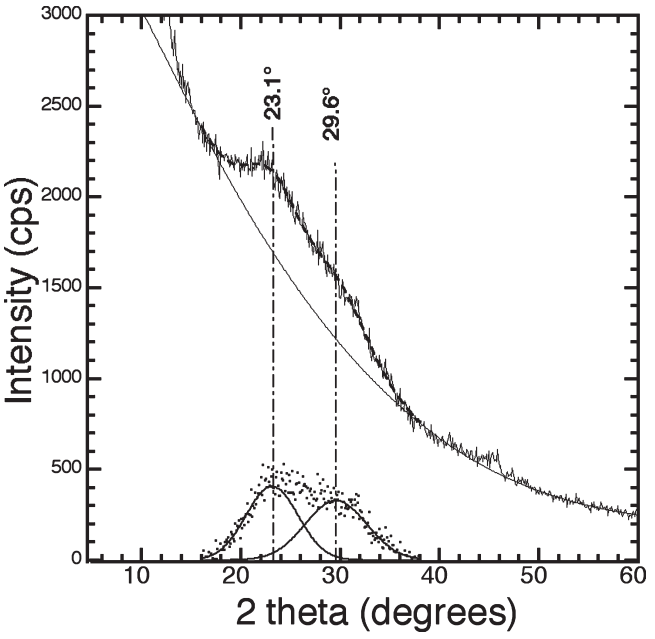

Figure 4. XRD pattern of the PPy film obtained by spin coating. Top: the raw diffraction pattern along with the background used and the result of the fit (dashed); bottom: the diffraction pattern after background subtraction (dots) with the two Gaussian peaks (lines) resulting from the fit. The presence of two peaks in this region result from a preferential orientation of the PPy film resulting from the spin-coating process.

diameter with the initial pyrrole content for samples left at rest for 3 months and extracted. Even after a long reaction time, the population of PPy particles remains rather monodisperse and nanometric, with an average hydrodynamic diameter that increases slightly from 150 nm to 300 nm as the amount of pyrrole increases from 20% to 100%. Parallel studies on the influence of stirring demonstrate that the quick mixing between phases A and B leads to particles smaller than those via the interfacial reaction, but it appears that the reaction time has almost no influence on the final size of PPy particles. (See Figure SI.2 in the Supporting Information.)

Particles obtained via this process are difficult to observe directly, because their size, shape, and composition lead to the merging of a continuous film upon drying. However, the influence of the liquid crystal on their shape can be confirmed by either some rodlike particles obtained after three months of reaction (see Figure SI.3a in the Supporting Information) or, more precisely, by the specific foliate structure obtained after natural drying of a drop of the aqueous suspension. (See Figures SI.3b and SI.3c in the Supporting Information.).

Structure of the Spin-Coated PPy Film. The XRD pattern of the film is displayed in Figure 4. This pattern exhibits a broad peak between 18° and 35°, which was fitted by two components, located at 23.1° (HWHM = 3.7°) and 29.6° (HWHM = 4.7°), respectively. Direct correlation with interactomic distances cannot be performed, because the Bragg law cannot be applied to amorphous compounds.[22] However, these values are similar to those already reported for PPy films in this region.[23,24] According to previous literature, the presence of two peaks could result from a preferential orientation of the PPy network resulting from the spin-coating process. Indeed, these two peaks can be observed with anisotropic structures marked by strong asymmetry in the low-angle scattering patterns.[25,26] This assumption will have to be confirmed by additional studies.

Different films were prepared by spin coating using either the aqueous suspension of PPy nanoparticles prepared in water according to Zhang,[11] dispersed under sonication, or the aqueous suspension obtained by our process. SEM observations of the bulk material (see Figures 5a and 5b) demonstrate that the spherical shape of these nanoparticles prevent them from forming a continuous film and only aggregates randomly dispersed on the surface could be observed. Unlike the previous material, spin coating of the aqueous suspension of nanosheets prepared in the SLC leads to a continuous and smooth film that perfectly covers the entire surface (see Figure 5c). Closer observation of this surface reveals a continuous matrix with some particles entrapped within (see Figure 5d).

Observation at higher magnification (Figure 6) confirms the existence of ~100 nm of remaining nanoparticles with a lamellar shape. These particles are the only objects that remain from the merging of the other particles, with this latter material creating the continuous film. This trend of natural fusion of lamellar objects with drying is particularly obvious when the aqueous suspension is allowed to dry naturally: a continuous film with a tile-like structure is observed with isolated particles remaining within (see Figure SI.4 in the Supporting Information). The AFM analysis confirms the excellent smoothness of this layer, with a root-mean-square (rms) roughness of ~4 nm (measured on a 5 μm × 5 μm surface) (see Figure 7).

For conductivity measurements, both low and high values of applied current resulted in inconsistent values of resistance (see Figure SI.5 in the Supporting Information). However, an applied current in the range of 0.003−0.001 μA gave consistent values of resistance. The average conductance deduced from these values was evaluated to 4.6×10^{-10} Siemens.

The conductivity σ is defined as

$$\sigma\ (\text{Siemens/cm}) = \frac{CL}{hw} \qquad (1)$$

where C is the lateral conductance of the film, L the spacing between the two-line probes, h film thickness, and

(22) (a) Guinier, A. *Théorie et Technique de la Radiocristallographie*; Dunot: Paris, France, 1964. (b) Fragnaud, P.; Prouzet, E.; Brec, R. *J. Mater. Res.* **1992**, *7*, 1839. (c) Bestaoui, N.; Prouzet, E.; Deniard, P.; Brec, R. *Thin Solid Films* **1993**, *235*, 35.

(23) (a) Buckley, L. J.; Roylance, D. K.; Wnek, G. E. *J. Polymer Sci. B* **1987**, *25*, 2179. (b) Saunders, B. R.; Murray, K. S.; Fleming, R. J.; McCulloch, D. G.; Brown, L. J.; Cashion, J. D. *Chem. Mater.* **1994**, *6*, 697.

(24) (a) Whang, Y. E.; Han, J. H.; Motobe, T.; Watanabe, T.; Miyata, S. *Synth. Met.* **1991**, *45*, 151. (b) Warren, L. F.; Walker, J. A.; Anderson, D. P.; Rhodes, C. G.; Buckley, L. J. *J. Electrochem. Soc.* **1989**, *136*, 2286.

(25) (a) Mitchell, G. R.; Geri, A. *J. Phys. D* **1987**, *20*, 1346. (b) Sutton, S. J.; Vaughan, A. S. *Synth. Met.* **1993**, *58*, 391.

(26) Mitchell, G. R.; Davis, F. J.; Legge, C. H. *Synth. Met.* **1988**, *26*, 247.

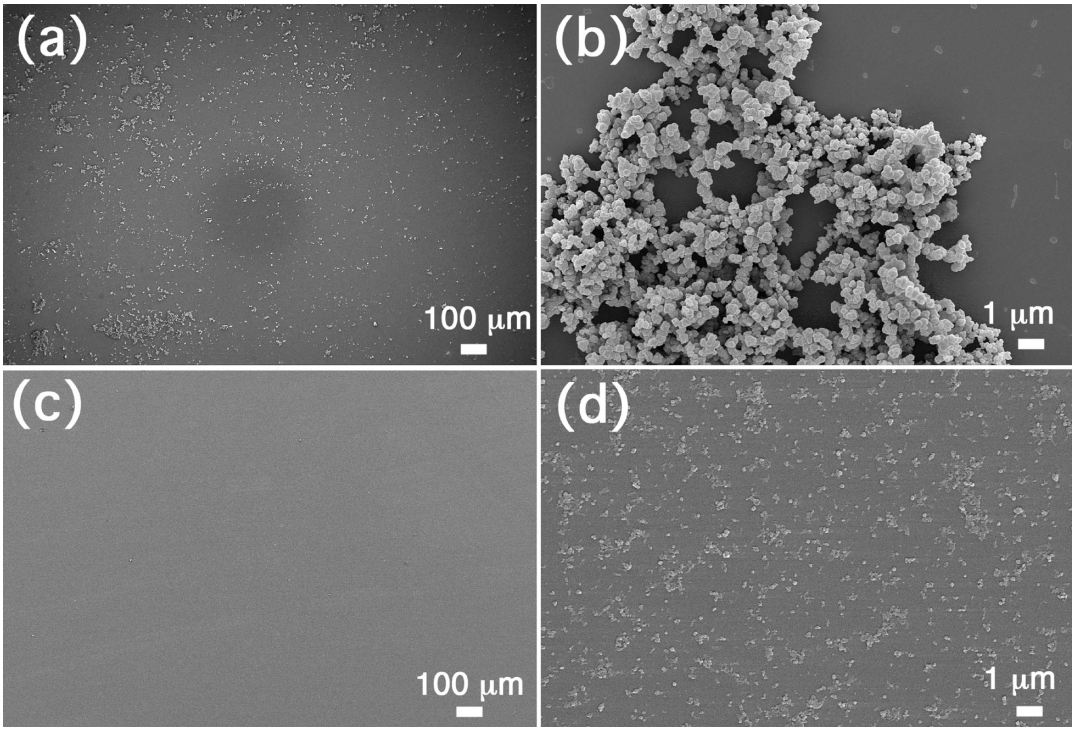

Figure 5. SEM micrographs of the PPy films prepared by the spin coating of an aqueous suspension of PPy nanoparticles prepared in (a,b) bulk water and (c,d) SLC. For the bulk material, the spherical shape of the nanoparticles prevents them from forming a continuous film, and they only form randomly dispersed aggregates on the surface, whereas the aqueous suspension of nanosheets prepared in the SLC leads to a continuous and smooth film that covers the entire surface perfectly.

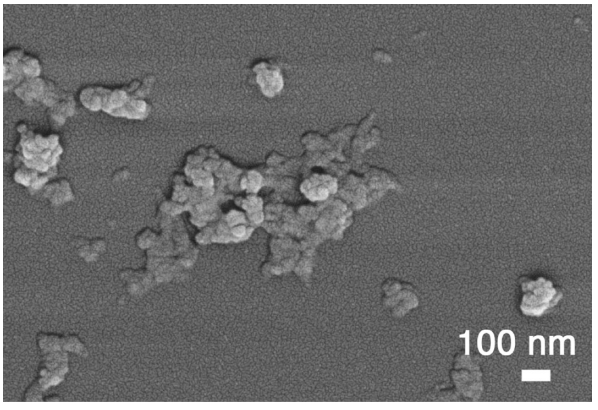

Figure 6. SEM micrograph of the PPy film obtained by spin coating from the aqueous suspension prepared in SLC. Observation at higher magnification confirms the existence of ~100 nm of remaining nanoparticles with a lamellar shape embedded in a continuous matrix.

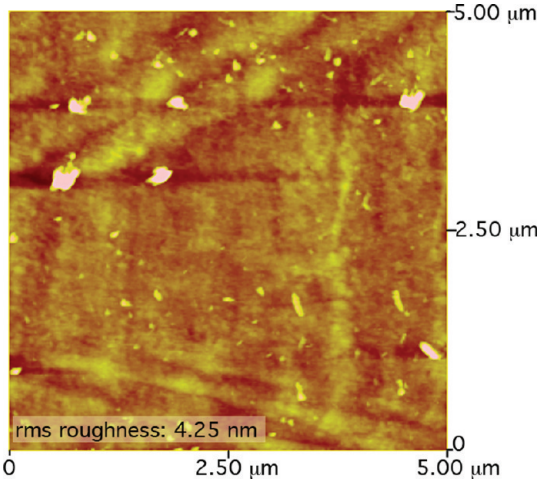

Figure 7. AFM observation of the PPy film, which confirms the excellent smoothness of the PPy layer, with a root-mean-square (rms) roughness of ~4 nm.

w the width of the total film. Our sample was 1 cm in width, the contact distance L was ~0.125 cm, and the average thickness h of the film prepared for the conductivity measurements by repeating the spin-coating operation 10 times was ~500 nm. This led us to a conductivity value of $\sim 1.15 \times 10^{-6}$ S/cm. This value can be compared with the conductivity reported by Mou et al. on polypyrrole films formed on mica by admicellar polymerization.[27] They reported a value of 2.6×10^{-3} S/cm for a 2.4-nm-thick CTAB−PPy film. Our PPy films are conductors that can be used for electrodeposition, as demonstrated thereinafter, but their current low conductivity (measured in the dry state) is still a drawback for an optimized process. However, the conductivity of PPy can be tuned by different methods such as ionic doping of formation of nanocomposites; this work is currently under study.[5,7,23,26,28]

Synthesis of ZnO Nanostructures. Uniform deposition of ZnO throughout the entire surface area of the substrate

(27) Mou, C.-Y.; Yuan, W.-L.; Tsai, I.-S.; O'Rear, E. A.; Barraza, H. *Thin Solid Films* **2008**, *516*, 8752.

(28) (a) Kuwabata, S.; Okamoto, K.; Yoneyama, H. *J. Chem. Soc., Faraday Trans. 1* **1988**, *84*, 2317. (b) Demets, G. J.-F.; Anaissi, F. J.; Toma, H. E. *Electrochim. Acta* **2000**, *46*, 547.

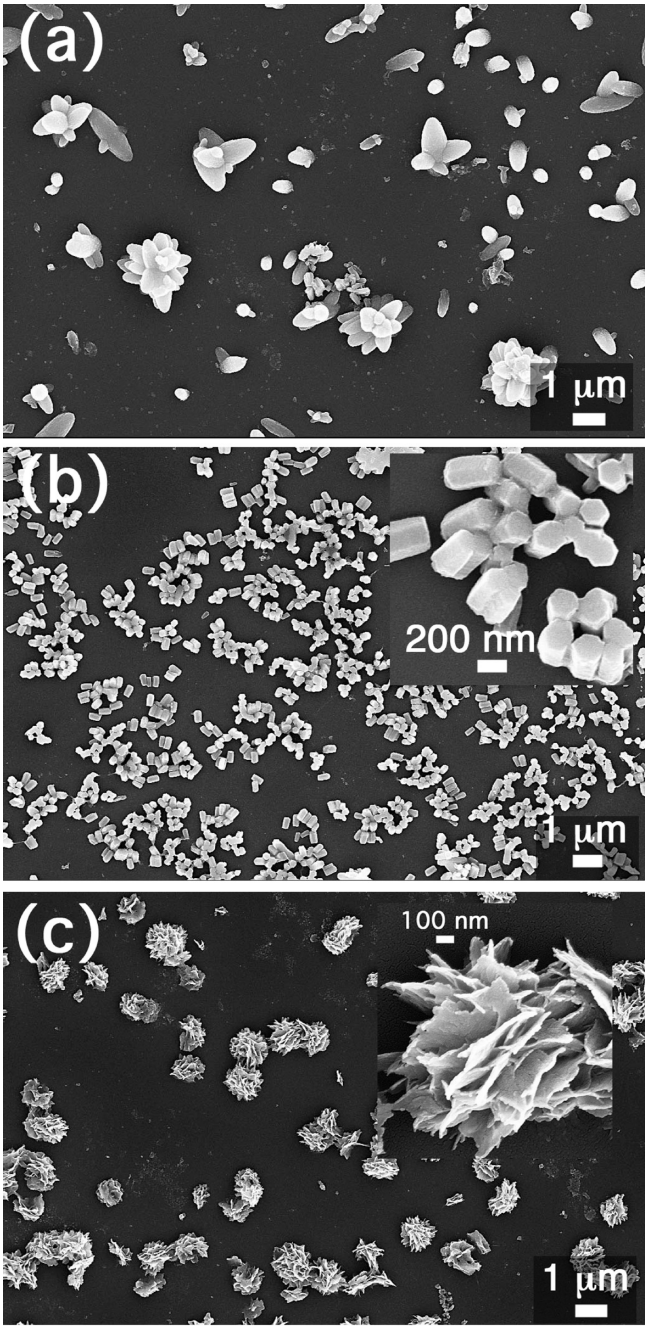

Figure 8. SEM micrographies of ZnO nanostructures formed onto the PPy film with 0.001 M solutions of zinc nitrate: (a) flower-like, (b) nanopillars, and (c) nanosheets.

was difficult. Most of the samples showed more deposition of ZnO nanoparticles near the clamped area, because of the low conductivity of the PPy sample. Figure 8 displays the structures obtained with the 0.001 M solution of $Zn(NO_3)_2 \cdot 6H_2O$ used for ZnO electrodeposition onto the PPy film. Different structures, similar to those obtained previously on PPy,[29] were observed in different regions of the substrate: flower-like (Figure 8a), hexagonal nanopillars (Figure 8b), and clusters of nanosheets (Figure 8c). These results demonstrate first that the PPy film can actually be used as an electrode for the electrodeposition of ZnO nanostructures.

Growth of specific nanostructures is highly dependent on local conditions such as the local voltage potential,[30] and a low conductivity can emphasize such heterogeneities. Note that the lower density of nanoflowers and nanopillars observed on a PPy-coated silicon substrate is due to the slow growth rate at a low electrolyte concentration (0.001 M). The final density of nanostructures is dependent on two parameters: concentration in electrolyte and reaction time. We set the deposition time to a given value—60 min—and we assume that increasing this deposition time would allow us to increase both the homogeneity and density of ZnO nanostructures.

In contrast to low-concentration electrodeposition, continuous layers of ZnO nanostructures were obtained with $Zn(NO_3)_2 \cdot 6H_2O$ (0.1 M) on both the PPy-coated silicon and PPy coated on gold-coated silicon wafers. This confirms the previous assumption regarding the higher growth rate within a given time, relative to a higher electrolyte concentration. We compared three types of substrates: PPy films spin-coated onto Si wafers (electrodeposition time of 60 min), gold-coated silicon wafer (electrodeposition time of 30 min), and PPy films spin-coated onto gold-coated silicon wafer (electrodeposition time of 60 min). Observations at low SEM magnification show that large surfaces of the substrate are covered by the ZnO nanostructures, with a quality and homogeneity of the grown layer increasing from the PPy film (see Figure SI.6a in the Supporting Information) to the PPy film coated onto gold (see Figure SI.6b in the Supporting Information) and finally to the gold-coated surface (see Figure SI.6c in the Supporting Information). Closer observations are reported in Figure 9. The ZnO grown on the PPy film alone exhibit(s) different shapes at different locations of the electrode: some areas are covered only with interlocked nanosheets structures (Figure 9a), whereas others present a composite structure with the interlocked nanosheets network and ill-defined nanopillars (Figure 9b). For the PPy film deposited onto the gold substrate, we observe a secondary growth of spherical aggregates made of nanoparticles onto the film of nanosheets structures. This secondary structure could result from the electrodeposition time (1 h), which is too long for this type of substrate, with regard to its better conductivity. The layer of ZnO nanostructures grown directly onto the gold substrate from a 0.001 M solution of zinc nitrate is very homogeneous, with regard to repartition and shape with only nanopillars (Figure 9d), as reported previously.[30] In contrast to low concentration electrodeposition, continuous layer of ZnO nanostructures is obtained at 0.1 M $Zn(NO_3)_2 \cdot 6H_2O$ on both the PPy-coated silicon and PPy coated on gold-coated silicon, because of the higher growth rate at a higher electrolyte concentration.

(29) Tian, L.; Qi, Y.; Wang, B. *J. Colloid Interface Sci.* **2009**, *333*, 249.

(30) Pradhan, D.; Leung, K. T. *Langmuir* **2008**, *24*, 9707.

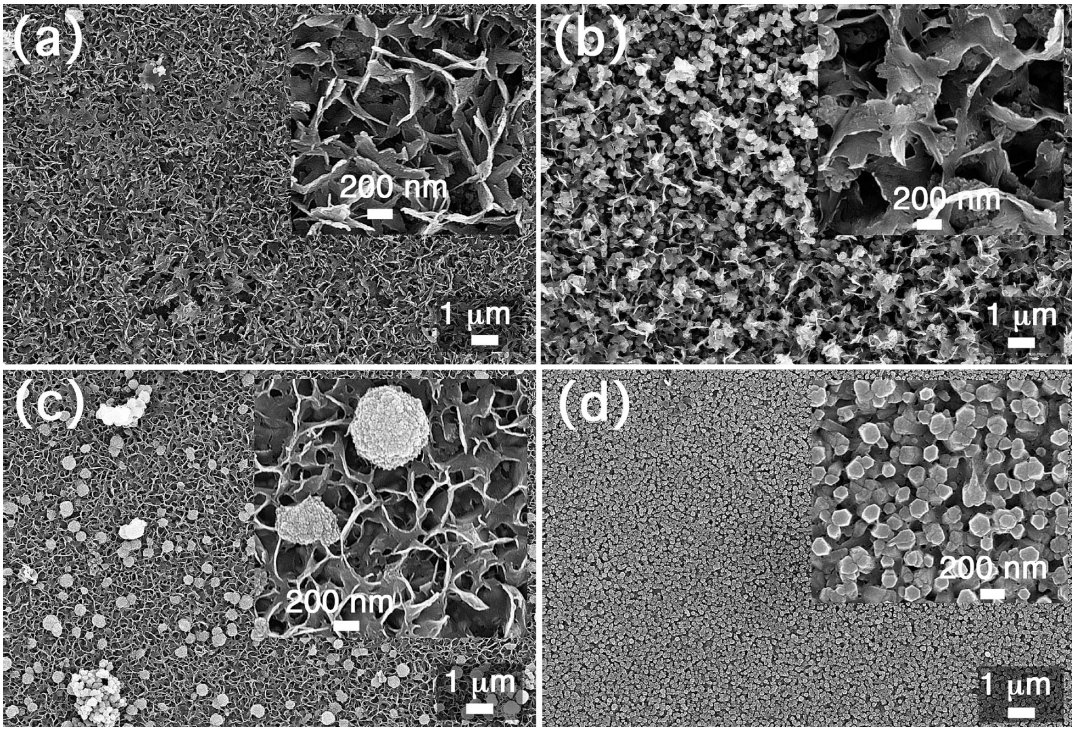

Figure 9. SEM micrographs of ZnO nanostructures formed with solutions of zinc nitrate: (a and b) grown onto the PPy film spin-coated on a silicon wafer with $Zn(NO_3)_2 \cdot 6H_2O$ (0.1 M), (c) grown onto the PPy film spin-coated on a gold-coated silicon wafer with $Zn(NO_3)_2 \cdot 6H_2O$ (0.1 M), (d) grown onto a gold-coated silicon wafer with $Zn(NO_3)_2 \cdot 6H_2O$ (0.001 M).

Conclusion

Integrative chemistry has opened a new field of development for materials prepared by soft chemistry methods, because it combines the assets of these methods (room temperature, aqueous medium) with the structuring properties of soft matter (such as swollen liquid crystals). We illustrated this method by preparing polypyrrole nanoparticles through an electroless process based on a simple chemical reaction conducted in the aqueous phase of these SLCs. The confinement provided by the liquid crystal leads to the formation of lamellar nanoparticles of polypyrrole that can be further extracted and stored as an aqueous suspension. The anisotropy of the particles so obtained, along with their small size, allowed us to create smooth thin films by a simple method such as spin coating. Although the conductivity of these films still must be increased by specific doping of formation of nanocomposites, they were sufficiently conductive to allow the electrodeposition of ZnO nanostructures with geometries that can vary as a function of the synthesis parameters. This study illustrates how this process could be expanded for the extension to other techniques of deposition, based on colloidal suspension: spray drying, dip coating, or inkjet printing.

Acknowledgment. The authors thank Dr. R. Sankar and Dr. H. Kleinke for help in conductivity measurements.

Supporting Information Available: Table SI.1 gives the synthesis parameters of the swollen liquid crystals that contain pyrrole (phase A). Figure SI.1 shows the fit of the autocorrelation function $G(\tau)$ for a suspension of PPy particles prepared in bulk water. Figure SI.2 shows hydrodynamic diameters deduced from the fit of the autocorrelation functions obtained from DLS analysis of the aqueous colloidal suspension of PPy particles obtained by quick stirring or interfacial reaction (unstirred) of phases A and B. Figure SI.3 shows SEM micrographs of PPy particles obtained with the 100% sample after three months. Figure SI.4 shows an SEM micrograph of a PPy film obtained by natural drying of the aqueous suspension of nanosheets prepared in SLC. Figure SI.5 shows the measurement of the conductance of the PPy film. Figure SI.6 shows SEM micrographs of ZnO nanostructures formed with 0.1 M solutions of zinc nitrate grown onto various silicon wafers. (All PDF Files.) This material is available free of charge via the Internet at http://pubs.acs.org.